Increased dependency of regional drought termination on landfalling tropical cyclones

Check for updates

Yaxin Liu[1], Xuezhi Tan [1,2]✉, Xinxin Wu [1], Xuejin Tan[1], Chengguang Lai[3], Huabin Shi[2,4] & Thian Yew Gan [5]

Landfalling tropical cyclones frequently occur with strong winds and heavy rainfall, providing substantial water resources. The positive impacts of tropical cyclones on drought alleviation and termination remain unknown. Here, we estimate the dependency of drought terminations on tropical cyclone rainfall through frequency analyses and event coincidence analysis. Results show that ~3% of the tropical cyclone-affected areas have experienced multiple drought events terminated by tropical cyclone rainfall from 1999 to 2021. Globally, tropical cyclone-terminated drought events averaged 1.12 annually and increased significantly by 1.92% per year. Increases were especially significant in the Arabian Peninsula, South Asia, and the northwest of Australia. Rainfall produced by tropical cyclones alleviates drought events more drastically than that by other weather systems, such as fronts, mesoscale convective systems, and atmospheric rivers. These findings underscore the adaptation of precipitation changes due to shifts in the timing and weather systems under a warming climate.

Landfalling tropical cyclones (TCs) are a major trigger of global economic and environmental devastation[1–3] due to TC hazards resulting from strong winds and heavy precipitation[4], but they may also bring some positive effects. TCs provide substantial hydrological benefits to reservoir-dependent regions through abundant precipitation, alleviating water scarcity and electricity shortages[5,6]. TCs play a role in redistributing heat from the tropics towards the poles, helping to regulate global temperatures and keeping polar (tropical) regions from being as cold (hot) as they would be otherwise[7]. They also enhance natural system productivity by delivering inorganic sediments to ecosystems[8]. TCs can support certain ecological processes like water provision, soil enrichment, and the restoration of ecological niches, contributing to biodiversity[5]. Landfalling TCs could bring a large amount of water resources for the impacted regions, which is especially beneficial for regions that have been experiencing severe droughts[9]. Successive occurrences of droughts and landfalling TCs could moderate the losses of natural and human ecosystems resulting from their individual adverse impacts[10]. For instance, Typhoon Saomai in 2005 effectively alleviated the drought in Shanghai[11]. Large landfalling TCs often terminate long-term regional droughts, so TCs show positive impacts on the water resources system,

which is seldom considered in climate adaptation. Temporally compound of droughts and TCs are not comprehensively investigated globally, despite some preliminary analyses of relations between TCs and droughts over the southeastern Atlantic United States[12] and China[13]. Droughts and TCs correspond to water deficit and surplus, respectively[10]. The successive occurrence of these two contrasting phenomena, relating to the dry to wet whiplash[14], has attracted communities of stakeholders in water resources management and disaster reduction and recovery. The lifespan of a TC is generally shorter than that of a drought event, so the timing of landfalling TCs is of great importance to drought terminations. Restoration of normal water quantities is viewed as drought termination and is a crucial phase in drought management[15]. Earlier drought termination is essential for mitigating destructive impacts and minimizing the need for costly interventions[16]. Rapid drought termination is a phenomenon of particular interest to water resource managers and municipalities, which is often defined as drought ending within 1 month[17]. Due to the increasing variability of precipitation[18], recent observations indicate an increasing abruptness in drought terminations[14,19] and climate change influences both the historical[14] and future drought termination[20]. For example, rapid drought

[1]Center of Water Resources and Environment, School of Civil Engineering, Sun Yat-sen University, Guangzhou, PR China. [2]Southern Marine Science and Engineering Guangdong Laboratory (Zhuhai), Zhuhai, PR China. [3]State Key Lab of Subtropical Building Science, School of Civil Engineering and Transportation, South China University of Technology, Guangzhou, PR China. [4]State Key Laboratory of Internet of Things for Smart City and Department of Ocean Science and Technology, University of Macau, Macao, PR China. [5]Department of Civil and Environmental Engineering, University of Alberta, Edmonton, AB, Canada. ✉e-mail: tanxuezhi@mail.sysu.edu.cn

termination events occurred frequently in the southeastern United States[21], and their underlying mechanisms are associated with various weather factors, including TCs[17] and anomalously high atmospheric vapor transport[22].

Frequent landfalling TCs during the warm seasons have been observed to alleviate droughts[10,12], but the occurrence frequency of moderate TCs decreased in the past four decades, despite increases in the occurrences of extremely heavy TCs[23]. The impact of intense TC rainfall on drought is particularly pronounced in coastal regions where population and infrastructure have grown rapidly[24], compared to inland regions[25]. Moreover, global TCs have poleward shifted[26] and are projected to poleward shifted under a warming climate[27]. However, global changes and variabilities of occurrence frequencies of successive occurrences of droughts and landfalling TCs remain unknown. Here, we identify regions where TC rainfall could terminate droughts and examine changes in the chances of regional drought termination due to TC rainfall. We show that drought terminations are becoming more dependent on TC rainfall in coastal regions, despite some regional differences.

Results
Changes in occurrences of TCs and drought termination events
The International Best Track Archive for Climate Stewardship (IBTrACS)[28] dataset shows that there were 2390 named TCs that occurred globally from 1999 to 2021, a period with stabilized satellite observation standards ensuring a long-term, reliable, and homogeneous TC track data. The global frequency of TCs shows an insignificant increase (0.17 per year) from 1999 to 2021, while a significant decrease from 1985 to 2022 (-0.38 per year) and 1951–2022 (-0.24 per year) (Supplementary Table 1). There are possible systematic biases in TC tracks during the pre-satellite era that may introduce spurious trends[29,30]. Long-term historical[31] and future projections[32] suggest an overall decline in the global frequency of TCs under a warming climate. These changes in TC frequency could have consequential effects on TC precipitation.

To identify regions where drought terminations could be caused by TC rainfall, we used the event coincidence analysis to evaluate the coincidence rate of drought terminations proceeded with large amounts of TC rainfall. The standardized precipitation index (SPI) is used to identify drought events ("Methods"). SPI-6 and SPI-12, estimated from precipitation at scales of 6 and 12 months, respectively, are considered to distinguish the effects of TC rainfall on terminating drought events of various temporal scales. A drought termination event is defined as one or more successive months of droughts with SPI values lower than -1.0 followed immediately by a month with an SPI value higher than -0.5. When the proportion of TC rainfall exceeds 50% of the total rainfall every 2 months, which is possibly the month of drought relief and the month of drought termination, we categorize that drought termination event as being predominantly influenced by TC precipitation (TCP). Three precipitation datasets of high spatial resolutions ($0.25 \times 0.25°$), CMORPH[33], PERSIANN-CDR[34], and ERA5-Land[35] were used to identify TC rainfall which are generally consistent in representing the total precipitation and TC precipitation, and their changes as well ("Methods" and Supplementary Fig. 1). In the event coincidence analysis, the percentage of drought events terminated by TC rainfall is evaluated and presented by the precursor coincidence rate. We count the number of grids and the associated number of times experienced TC rainfall or drought terminations with the unit of *grid times*.

A drought termination event occurred across the Pacific coast of Mexico (centered at 106.125°W, 23.125°N) from May to June 2021 due to two consecutive TCs, including Dolores and Enrique (Fig. 1a). In May, the SPI-12 value at this location was -1.08, indicating a moderate drought. By June, the SPI-12 had risen to 0.18, signifying the alleviation of the drought. This process represents a drought termination event. During these 2 months, TCP amounted to 165.2 mm (Fig. 1b), which is 89.78% of the total precipitation (183.2 mm). Since TC rainfall contributed to more than 50% of the total precipitation, this event is classified as a TC-DT event. Based on TC track data, filtering the daily rainfall during these 2 months at this location to identify TC-related rainfall (Fig. 1c). The result shows that the

precipitation on June 19, 20, 27, 28, 29, and 30th, 2021, resulted from TCs, including Dolores and Enrique. The locations, intensities, and total precipitation during the passage of the TCs are shown in Fig. 2.

In the areas affected by TCs, the frequency of drought termination (DT) events shows a significant decrease (Fig. 3a), while the number of TCs that trigger DT events (DT-TC) shows a significant increase. Thus, the occurrence of DT events induced by TCs shows a pronounced increase. From 1999 to 2021, the trend analyze results derived from different datasets and SPI calculations of various temporal scales are generally consistent (Supplementary Table 1), with the exception of the SPI-6 results for DT-TC, which show an insignificant decrease. For the period from 1985 (1951) to 2022, both TC and DT events show a significant decrease, while TC-DT events show an increase. Therefore, in areas affected by TCs, the importance of TCs for DT has been increasing due to the increasing likelihood of TCs followed by drought events.

Probability of drought termination by TC rainfall
There were 539 TCs (22.55% of the total) that played a role in DT events. There is a statistically significant increase in the number of TCs by 1.92% per year that contributes to DT (Fig. 3b). The proportion of TCs that have a major effect on DT events to the total number of TCs also shows an increasing trend in all datasets (Supplementary Table 1). To assess the impacts of TC on DT, we compute the coincidence rate from binary variables from the occurrence of high TC rainfall and DT events (see "Data and Methods"). Event coincidence analysis shows that in most coastal regions, the coincidence rates are greater than 0 and some regions show values of the precursor coincidence rate exceeding 0.5 (Fig. 3c). This indicates a high percentage of drought events terminated by high TC rainfall in these hotspot regions, including the east and west of North and Central America (Fig. 3d), the Arabian Peninsula and South Asia (Fig. 3e), the regions of Southeast and East Asia (Fig. 3f), and the northwest of Australia (Fig. 3g). TC-DT events are mainly distributed near the coastline where TCs frequently go through and bring about high precipitation (Supplementary Fig. 7). Since the interior regions could more frequent with drought events in the season of TCs than the very coast regions, drought events terminated by TC rainfall have also occurred frequently in interior regions (Fig. 4). TC-DT events over the Middle East mainly occurred on the east coast near the Indian Ocean. TC-DT events over Asia mainly occurred in coastal areas near the Pacific Ocean. TC-DT events over North and Central America mainly occurred on the east and west coasts, and TC-DT events over Australia mainly occurred on the west side of the continent.

For the timing of TC rainfall and DT events, TC rainfall occurs mostly from August to November in the Northern Hemisphere, and from December to March in the Southern Hemisphere (Fig. 3h). DT events over the regions impacted by TC rainfall are more widely distributed. There is no significant seasonal difference between the Northern and Southern Hemispheres (Fig. 3i). DT events mostly occur from April to June in East and Southeast Asia, from December to January in the Middle East and South Asia, and in the Southern Hemisphere from November to February. The peak time of DT events and TC rainfall are not well consistent and thus their coincidence rates are mostly lower than 0.3 (Fig. 3c). Note that there are seasonal changes in TC rainfall proportion to the annual total precipitation, in which TCs produce less precipitation in September in the Northern Hemisphere while higher precipitation in other months in both the Northern and Southern Hemisphere (Fig. 3h). There could be higher chance of TC rainfall to terminate droughts in regions of increasing TC rainfall.

Increased droughts terminated by TC rainfall
There are ~3% of the global TC-affected land area ($1.41 \times 10^6 \text{ km}^2$) where more than one drought event terminated by TC rainfall from 1999–2021 (Supplementary Table 2). These regions are mostly located at the populated coast areas in Asia, North America and Oceania, which are further selected to show the impacts of TC rainfall on DT (Fig. 4). The number of DT events shown by the SPI-12 and SPI-6 are 2.88 and 6.67 times, and those caused by TC rainfall are 1.12 and 1.20 times on average within the considered grids,
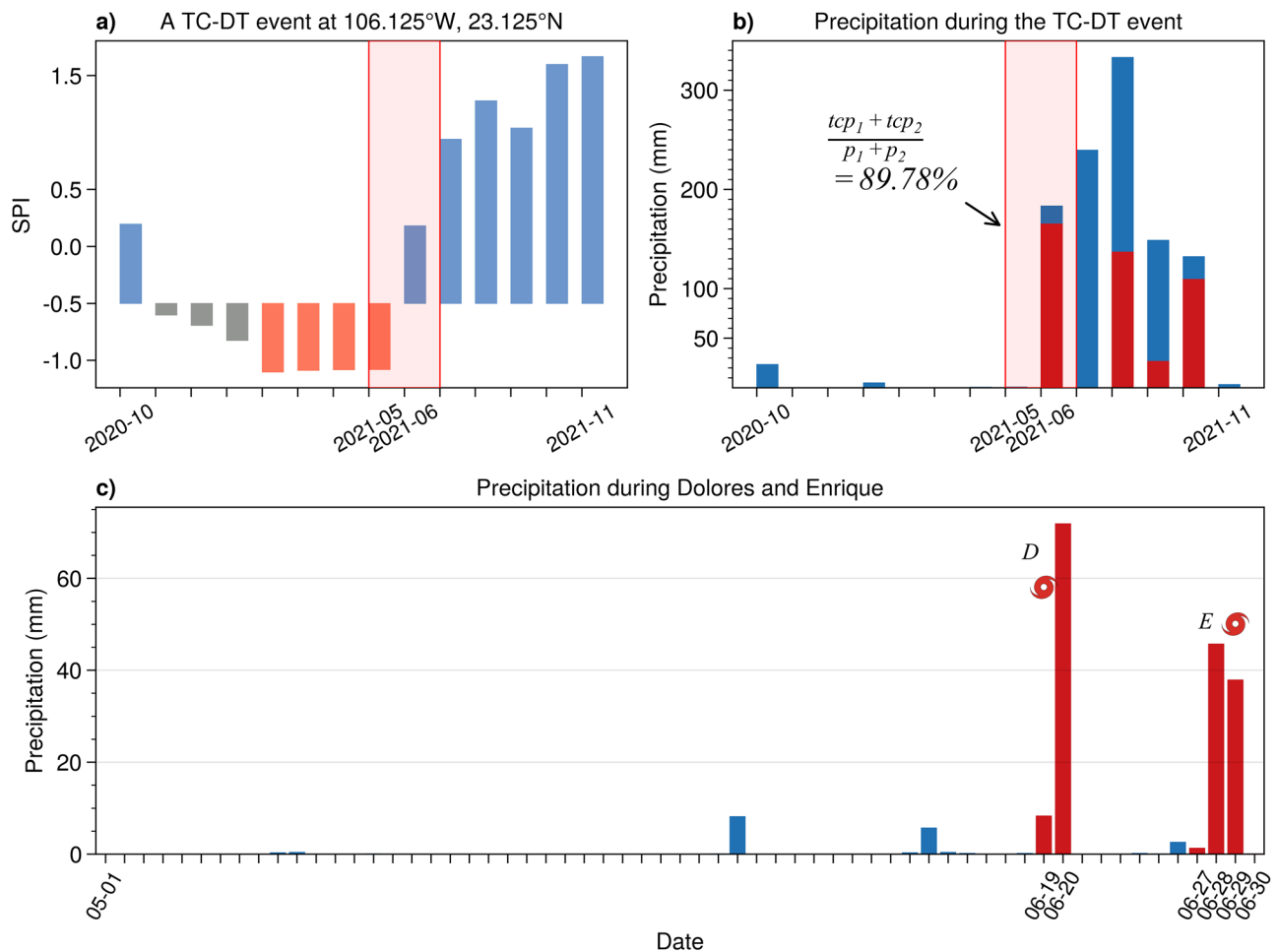
Fig. 1 | Changes in SPI-12 and monthly precipitation in an exemplary TC-DT event occurred across the Pacific coast of Mexico (centered at 106.125°W, 23.125°N). a SPI-12 value changes during a TC-DT event (light red shaded area). Total precipitation (p_1, p_2, blue bars) and TCP ($tcp_1 = 0$, tcp_2, red bars) in the first month and second month during the TC-DT event period. **b** TCP accounts for 89.78% of total precipitation in the 2 months. **c** Daily precipitation from May to June during the TC-DT event. The red bar indicates that the precipitation on that day is TCP (with a red TC icon above).

respectively. The average numbers of these events for 1999–2021 calculated by the three datasets are very close, slightly lower than the average value for the 1985–2022 period, with the highest average value for events in the 1951–2022 period (Supplementary Table 3). Similar to the results of the event coincidence analysis, DT events caused by TC rainfall mostly occurred in the four hotspot regions. The spatial distribution of TC-DT events obtained from the three precipitation datasets is consistent, except for the slight differences in the absolute number of TC-DT events. Although the lengths of PERSIANN-CDR (1985–2022) and ERA5-Land (1951–2022) are longer than that of the CMORPH dataset (1999–2021), the absolute numbers and changes in the TC-DT events in the same period of 1999–2021 shown by the CMORPH, PERSIANN-CDR, and ERA5-Land datasets are consistent (Fig. 4 and Supplementary Fig. 2). To examine changes in the number of TC-DT events, we conduct the Poisson regression to identify its trend on the global scale (Fig. 5a and Supplementary Fig. 3a). The annual global number of TC-DT events at the 12-month scale ranges from 0 to 240 *grid·times*. All three precipitation datasets indicate that the number of TC-DT events show a statistically significant increase from 1999-2021 with increasing rates of 2.22%, 1.24% and 7.56% per year obtained from the CMORPH, PERSIANN-CDR, and ERA5-Land datasets, respectively (Fig. 6), which may be part of natural variability. In recent decades, TCs of greater intensity and precipitation occurred more frequently, while TCs of low intensity occurred less frequently[36,37]. Therefore, there is a significant increase in the occurrences of TC-DT events for severer droughts. The annual number of DT events ranges from 0 to 500 *grid·times* in the study

region. The annual proportion of TC-DT events to DT events ranges from about 15 to 60%, indicating that TC rainfall plays a key role in terminating droughts. The proportion of TC-DT events to DT events shows an insignificant increasing trend. The number of DT events show an insignificant (significant) increasing trend for CMORPH (PERSIANN-CDR and ERA5-Land) from 1999 to 2021, although it is significantly decreasing shown by the PERSIANN-CDR dataset from 1985 to 2022 and the ERA5-Land dataset from 1951 to 2022. These discrepancies may be attributed to inherent differences in the precipitation data themselves and the constraints of the study period.

For short-scale droughts shown by SPI-6, the trends of the number of TC-DT and DT events are similar to those shown by SPI-12, except the trend of DT events is mainly decreasing (Fig. 6). Since TCs tend to bring short-term heavy precipitation, TC rainfall is more likely coincident with severe droughts lasting a long period, and thus TC rainfall more frequent with DTs at longer time scales. From the long-term perspective, the number of TC-DT significantly increased (decreased) from 1985 to 2022 and 1951 to 2022 for the long-scale (short-scale) droughts (Fig. 6). For the four hotspot regions of TC-DT, the Arabian Peninsula and South Asia (Fig. 5c), and Australia (Fig. 5i) show a statistically significant increase in the number of TC-DT events. All datasets and 3-month results (Supplementary Fig. 4) show a consistently and statistically significant increase for the two regions. For the number of DT events, the Arabian Peninsula and South Asia, and Australia (North and Central America) show a statistically significant increase (decrease). Southeast and East Asia shows inconsistent trends
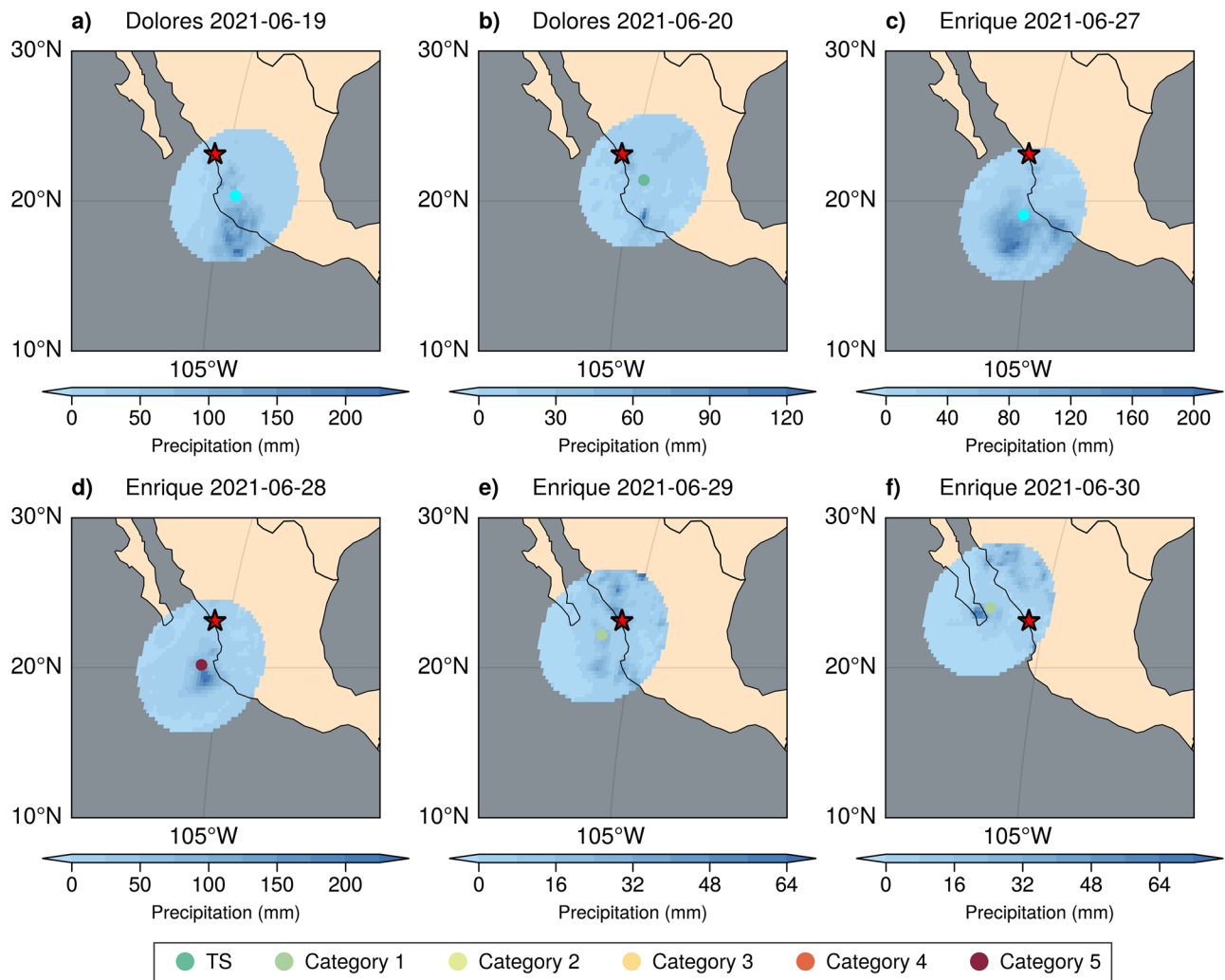
Fig. 2 | The location, intensity, and precipitation distribution of TCs in a TC-DT event. Precipitation produced by Tropical cyclones Dolores and Enrique shown in Fig. 1c are spatially and temporally shown for Tropical cyclones **a** Dolores on 2021-06-19, **b** Dolores on 2021-06-20, **c** Enrique on 2021-06-27, **d** Enrique on 2021-06-28, **e** Enrique on 2021-06-29, and **f** Enrique on 2021-06-30. Tropical cyclone precipitation is identified with a radian of 500 km around the center of TCs on that day. The color of the tropical cyclone center shows the categories of Saffir–Simpson Hurricane Wind Scale according to the maximum sustained winds on that day. The red pentagram is the exemplary location where one TC-DT events occurred (106.125°W, 23.125°N).

obtained from the three different datasets. Both the number of DT events and TC-DT events in the Arabian Peninsula and South Asia increased significantly from 1999 to 2021 (Fig. 5c). The strong vertical wind shear in the north of the Indian Ocean is not conducive to the transport of updrafts[38], so the number of TCs impacting the Middle East is usually small. However, when the vertical wind shear is weakened in the transition from spring to summer, or from fall to winter[39], strong TCs could produce a large amount of precipitation. For example, the super typhoon Chapala occurred in the Arabian Sea in October 2015[40] resulted in TC-DT events across large areas of the Middle East.

The number of TC-DT events in Southeast and East Asia shows an insignificant increase from 1999 to 2021 (Fig. 5e), while DT events show an insignificant decrease. The proportion of TC-DT to DT events shows an insignificant increase from 1999 to 2021 (Fig. 5f). However, PERSIANN-CDR (ERA5-Land) shows a significant decrease in TC-DT and DT events from 1985 to 2022 (1951–2022) in East and Southeast Asia (Fig. 6). While the number of TC-DT events account for a high and increasing proportion of the number of DT events (Fig. 5h), the number of DT events show a decreasing trend in North and Central America (Fig. 5g). These indicate that TCs have an increasing impact to terminating droughts in North and Central America. In Australia, the number of TC-DT events and DT events show a significant increase, and the results from 1999 to 2021 obtained from

the three precipitation datasets are consistent (Figs. 5i, j, 6). The 3-month results show a more significant increase in TC-DT events and DT events in the different SPI calculations of various temporal scales (Supplementary Fig. 4).

For short-term drought calculated from SPI-6 (Fig. 6) in the Arabian Peninsula and South Asia, the number of TC-DT events shows a significant increase, while the number of DT events shows different significant trends for the three datasets. The three datasets all show an insignificant increase of the annual proportion of TC-DT to DT events in the Arabian Peninsula and South Asia. The sign of the most significant trends of the number of TC-DT and DT events in other regions is inconsistently shown by the three precipitation datasets, which is partly caused by short time series from 1999 to 2021. The number of drought events, lasting continuously three or more months with SPI-6 lower than −1.0 in these 3-month ("Methods" and Supplementary Fig. 4) also show a significant increase in Global, the Arabian Peninsula, South Asia, and Australia, while a significant decrease in Southeast and East Asia and North and Central America.

For changes in the long period from 1985 to 2022 and 1951 to 2022, the number of TC-DT events shows a significant increase globally for long-term drought, even though the number of DT events show a significant decrease shown by the PERSIANN-CDR and ERA5-Land datasets for both the short- and long-term droughts. These changes for the long-term droughts are also
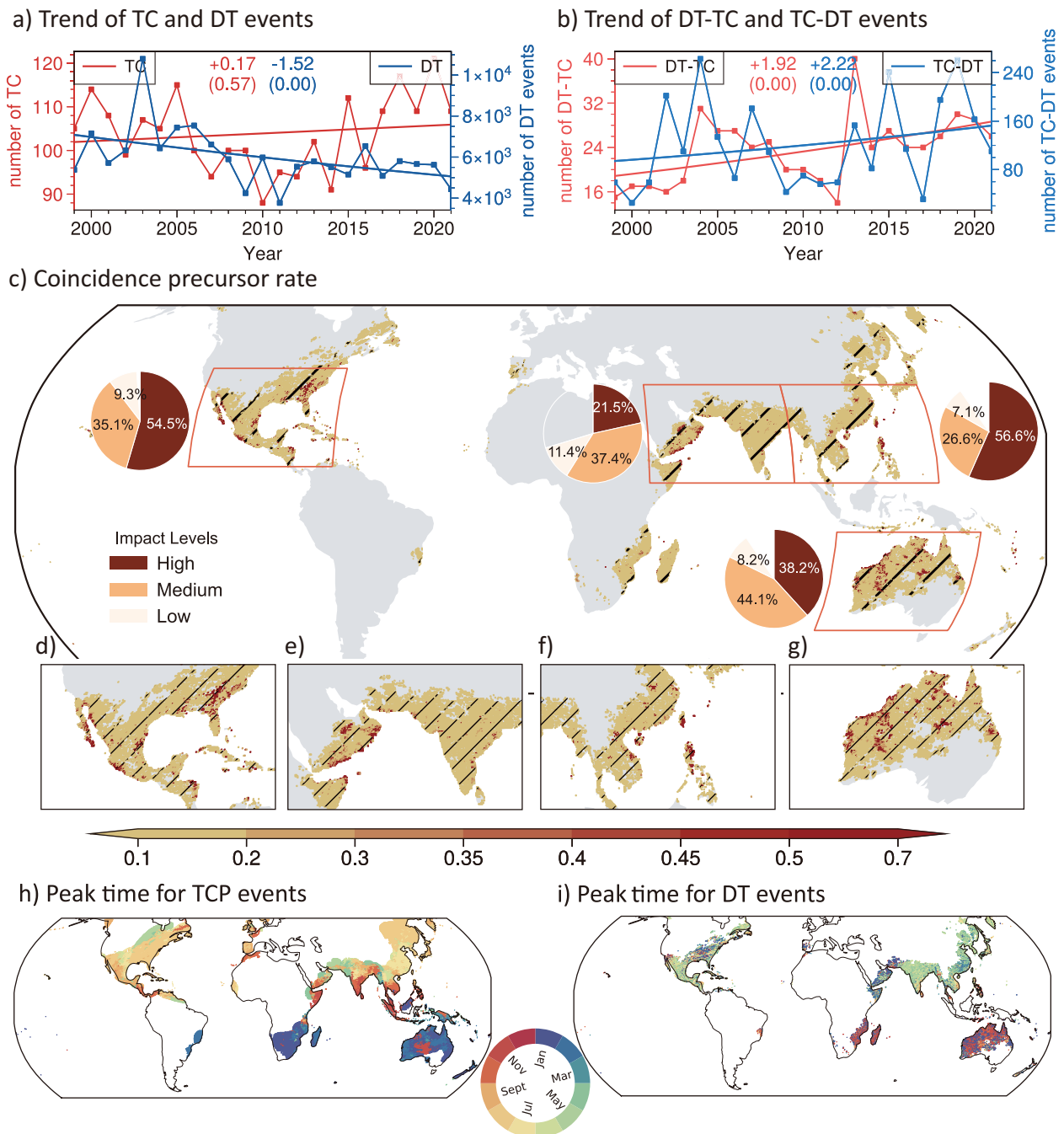
Fig. 3 | Concurrences of TC rainfall and drought termination events. a trend of the number of named TCs (TC, red lines) and terminate drought (DT, blue lines) events derived from SPI-12 using CMORPH precipitation dataset for the area affected by TC as shown in Supplementary Fig. 5. The top number inserted in the plots is the slope of Poisson regression (+0.17% and −1.52% per year), and the number in parentheses (0.57 and 0.00) is the significance level of the Poisson regression. b the same as a, but for named TCs that caused DT events (DT-TC, red lines) and DT events caused by high TC rainfall (TC-DT, blue lines). c global distribution of precursor coincidence rate of high TC rainfall events to drought termination events. The pie chart shows the degree of TC impact on the land part of each hotspot area. High TC rainfall events are defined as the combined TC rainfall of two neighboring months exceeds 50% of the total precipitation for those 2 months. A climatological

transition at the end of a drought event from the first month of SPI less than −1.0 to the following month of SPI larger than −0.5 is regarded as a DT event. The concurrence of high TC rainfall events and drought termination events is defined as a tropical cyclone-related drought termination (TC-DT) event. Slash lines indicate regions of statistically significant precursor coincidence rate. The red boxes show the four hotspots of high concurrence probabilities of high TC rainfall events to drought termination events, including the east and west of North and Central America (d), the Arabian Peninsula and South Asia (e), the Southeast and East Asia (f), and the northwest of Australia (g). h spatial distribution of the peak month of high TC rainfall, and i the spatial distribution of peak month of drought events from 1999 to 2021, respectively. Only regions impacted by TCs are shown in the maps and quantitatively analyzed for drought termination.

shown in the two hotspot regions, including North and Central America, and Australia. However, Southeast and East Asia show a significant decrease in both the number of TC-DT and DT events, while the Middle East and South Asia show a significant increase in the number of TC-DT and DT events.

Effects of TC rainfall on alleviating drought
To further distinguish the effects of TC rainfall on drought, we also examine the effects of TC rainfall on drought alleviation, although the drought events may not be terminated by TC rainfall. We classified DT events into two

Fig. 4 | Spatial distribution of the number of drought termination (DT) events and those caused by high rainfall (TC-DT). Results are derived from the droughts identified with SPI-12 using CMORPH precipitation dataset. **a** Global distribution of TC-DT and DT events. The red boxes show the four hotspots of high concurrence probabilities of high TC rainfall events to drought termination events, including the east and west of North and Central America (**b**), the Arabian Peninsula and South Asia (**c**), the Southeast and East Asia (**d**), and the northwest of Australia (**e**).
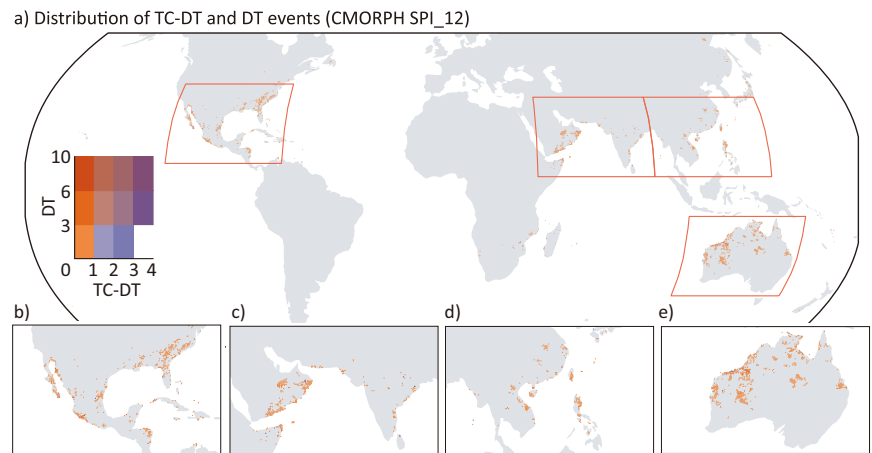
types, i.e., TC-DT and No_TC-DT, which are terminated by other types of precipitation such as fronts, mesoscale convective systems, and atmospheric rivers[17,41]. Figure 7 shows SPI-12 values in the first and second months of NoTC-DT and TC-DT events. SPI-12 values in the first month of the TC-DT events are lower than those of No_TC-DT events, although SPI-12 values in the first month of both NoTC-DT and TC-DT events are less than −1.0. This implies that TC rainfall terminates severe drought events efficiently. Furthermore, SPI-12 values (mostly SPI-12 > 0) in the second month of TC-DT events are significantly higher than those of No_TC-DT events, so TC rainfall generally shifts the drought to very wet conditions (SPI-12 > 1). All precipitation datasets draw a consistent conclusion. It remains true for droughts identified with SPI-6 of short time scales (Supplementary Fig. 5). Shifts in SPI values in TC-DT events across the four hotspot regions are similar to those for global regimes, although SPI values in North and Central America (Fig. 7e) and the Arabian Peninsula and South Asia (Fig. 7c) are higher after DT than those in other regions (Fig. 7d, f). These show that TC rainfall is more effective in alleviating drought than other types of precipitation in the four hotspot regions, especially for North and Central America and the Arabian Peninsula and South Asia.

We further analyze the weather conditions for each TC-DT event, and obtain the composite values of the maximum wind speed, mean wind speed, TC precipitation, and the number of days experienced in TCs for all TC-DT events (Fig. 8). The maximum wind speed and precipitation occurred in the first month when SPI ranges from −3.5 to −3.0, and the second month when SPI ranges from 0.5 to 1.0 (Fig. 8a, c). The maximum wind speed is 108.75 knots (Fig. 8a), and the maximum mean wind speed is 76.67 knots (Fig. 8b). The maximum TC total rainfall within the 2 months of a TC-DT event is 573 mm. These maximum values are basically located in the upper left corner of subplots in Fig. 8 with extremely low (high) SPI in the first (second) month of that DT events. This indicates that TCs with higher intensity and greater rainfall are concurrent to DT of more severe shifts in drought regimes. As expect, intensive TCs are more efficient to alleviation drought events. The days of TC experienced for all TC-DT events are calculated on each grid, with a maximum value of 7.96 days in the first month when SPI ranges from −1.5 to −1.0, and from 0.5 to 1.0 in the second month (Fig. 8d). TC days in the upper left corner are the highest of 6 days. Results of weather regimes for TC-DT events identified with the three precipitation datasets and time scales are similar in all four hotspot regions to Global (Supplementary Fig. 6). TCs of high intensity and great precipitation are concurred with extremely dry (wet) before (after) the DT.

Discussion

In this study, we report a global rise in the number and proportion of TCs which terminate drought events over the past two decades, based on observational TC tracks and multiple precipitation datasets. Approximately 3% of the TC impacted land area has experienced more than one drought

event terminated by TC rainfall from 1999–2021, and the annual average number of drought events terminated by TC rainfall is 1.12 times, with an increasing rate of 1.92% per year. Because the number of DTs occurred shows significant decreases and that of TCs shows no significant change, the increases in TC-DT result from their concurrences, partly due to their changes in timing. Because TCs mainly affect coastline regions around the world (Supplementary Fig. 7)[24], four hotspot regions show a high probability of TCs terminating regional droughts, including the east and west of North and Central America, the Arabian Peninsula and South Asia, the Southeast and East Asia, and the northwest of Australia.

Both the total TC rainfall and its proportion to regional total rainfall have increased, so the contribution of TC rainfall to regional water resources, and the chance of TC rainfall to terminate regional droughts as well increased from 1999 to 2021. Therefore, there is a significant increase in both TC-DT and DT events in the TC-impacted regions, especially in the Arabian Peninsula and South Asia, and the northwest of Australia, although the proportion of TC-DT to DT events shows an insignificant increasing trend. It should be note that the quantification of concurrent DT and TC rainfall is subjected to the observational precipitation uncertainties arising from the large spatiotemporal variability and rareness of the concurrence samples. However, the results derived from different datasets for different regions are minorly different (Fig. 6 and Supplementary Fig. 4), and the changes in their concurrence are consistent. A long and consistent observation of high spatiotemporal TC and precipitation data is required to show the spatial variations of changes in the occurrences of DT events caused by TC rainfall[37]. Moreover, whether changes in occurrences frequencies of TC-DT events result from natural variabilities (e.g., El Niño Southern Oscillation and North Atlantic Oscillation) or external forcings such as anthropogenic impacts on climate change should be further investigated to improve the underlying mechanisms for occurrences of TC-DT events.

Due to the high intensity of TC rainfall[42,43], compared to other precipitation systems such as fronts, mesoscale convective systems, and atmospheric rivers[17,41], the drought regimes shift more drastically before and after the TC rainfall, as shown by the comparison of SPI changes of drought events whether terminated by TC rainfall. Furthermore, the large amounts of rainfall produced by landfalling TCs alleviate drought more completely. Empirical evidence suggests that TCs may postpone drought onset through direct hydrological recharge via precipitation inputs and soil moisture augmentation, as well as indirect microclimatic modulation through temperature reduction and humidity elevation[44]. TC can significantly increase soil moisture in some areas, thereby reducing the possibility of drought[45]. In addition, the precipitation brought by TC can also alleviate the intensity of drought. Even if drought still occurs in the end, its severity may be reduced due to TC precipitation[44]. These factors can work together to delay the onset of drought or weaken the intensity of drought[45]. However, the specific features for individual TC-DT events, such as their duration, extremity, and spatial coverages, are not analyzed in detail due to large variations between
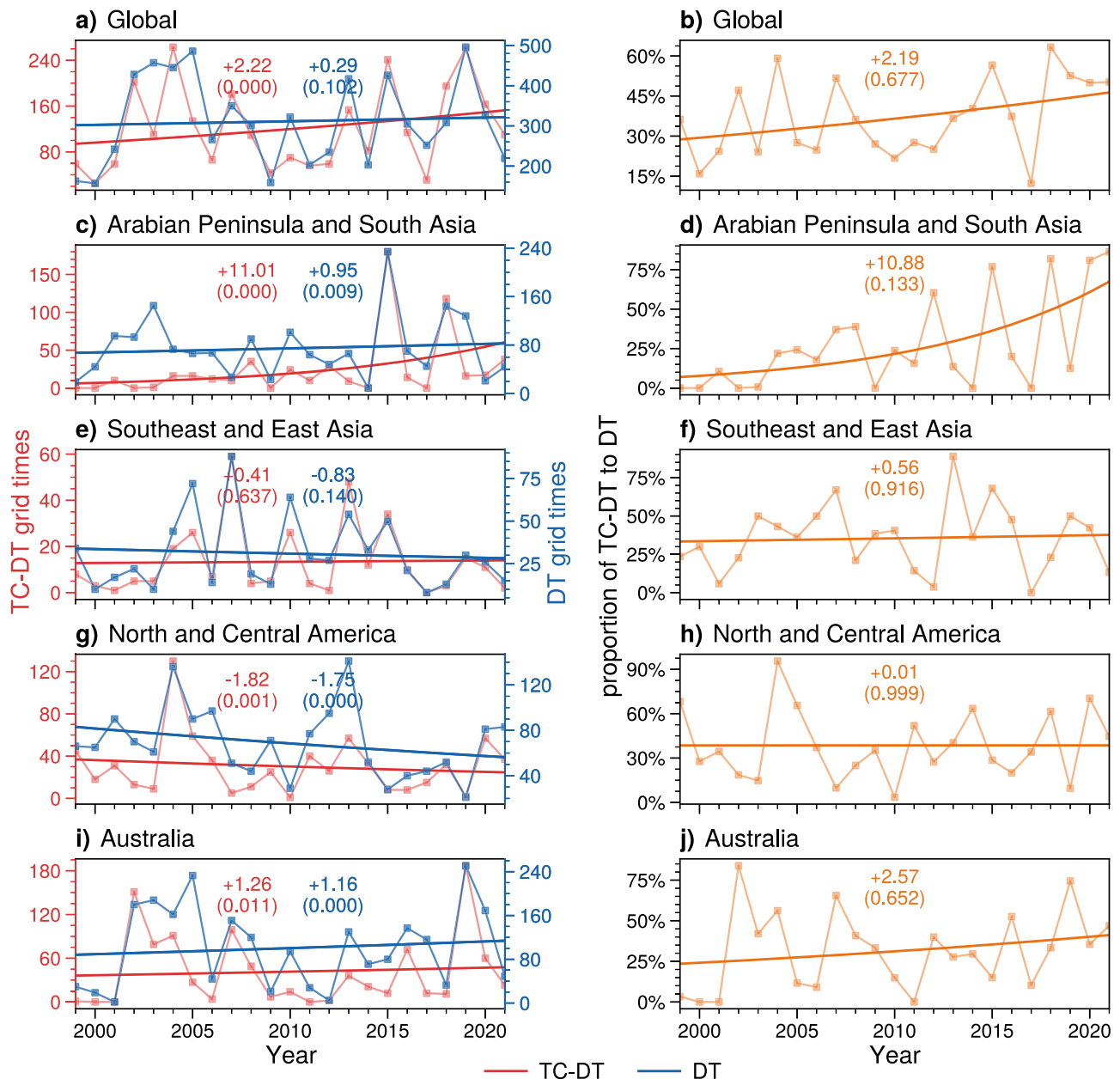
Fig. 5 | Annual changes in the number of drought termination (DT) events and those caused by high rainfall (TC-DT). Poisson regression results for the number of TC-DT and DT events (**a, c, e, g,** and **i**) and the proportion of TC-DT events to DT events (**b, d, f, h,** and **j**) derived from SPI-12 using CMORPH precipitation dataset for global (**a, b**) and the four hotspot regions, including the Arabian Peninsula and South Asia (**c, d**), the Southeast and East Asia (**e, f**), the east and west of North and Central America (**g, h**), and the northwest of Australia (**i, j**). Numbers in the first and the second row inserted in the subplots indicate the changing rate (%) and the significance of the changing rate, respectively.

real TC-DT events and a lack of a method to generalize their features. The machine learning method could be effective to investigate detailed features for each TC-DT events in further studies[46].

The connections between TC rainfall and regional droughts are only considered in very local regions previously[44], but the enhanced role of TCs in mitigating drought motivates us to make full use of the water resources benefit of TCs[9] while conducting timely adaptation actions to TC-induced hazards[24]. Water resources management by optimal reservoir operation has to consider the risk of both water resources and hazards to efficiently regulating TC rainfall-induced streamflow[47]. Our findings also have implications for ecosystem and human environmental changes, as both TCs and droughts could alter ecosystem and environmental functioning, such as food security, health, and biodiversity[48].

Methods
Tropical cyclone rainfall
Precipitation data of high spatiotemporal resolution are required to accurately identify precipitation rates due to TCs and regional drought characteristics[49–52]. We utilized three daily precipitation datasets. The first dataset is the Precipitation Estimation from Remotely Sensed Information using Artificial Neural Networks-Climate Data Record (PERSIANN-CDR) which provides daily precipitation estimates at a resolution of $0.25 \times 0.25°$ for the latitude band 60°S–60°N from 1983 to 2022[34]. The second dataset is derived from the Climate Prediction Center morphing method (CMORPH)[33], providing global daily data (60°S–60°N) at a resolution of $0.25 \times 0.25°$ from 1998 to 2021[53]. The third dataset is ERA5-Land released by the European Center for Medium-Range Weather Forecasts, offering daily

		CMORPH 1999-2021		PERSIANN-CDR 1999-2021		PERSIANN-CDR 1985-2022		ERA5-Land 1999-2021		ERA5-Land 1951-2022	
		SPI_12	SPI_6	SPI_12	SPI_6	SPI_12	SPI_6	SPI_12	SPI_6	SPI_12	SPI_6
Global	TC-DT	+2.22	+0.75	+1.24	+0.79	+1.07	-0.28	+7.56	+1.50	+0.31	-0.13
	DT	+0.29	-0.08	+0.40	-1.24	-0.80	-1.26	+2.60	+0.21	-0.09	-0.12
	proportion	+2.19	+0.81	+0.89	+2.15	+1.27	+0.23	+4.20	+1.49	+0.34	-0.05
Arabian Peninsula and South Asia	TC-DT	+11.01	+7.22	+11.24	+10.25	+6.44	+1.90	+9.53	+11.94	+0.63	+0.51
	DT	+0.95	+0.45	+2.59	-1.49	+0.78	-1.30	+1.63	-0.14	+0.28	+0.00
	proportion	+10.88	+7.68	+9.08	+8.64	+2.47	+2.10	+4.79	+10.75	+0.13	+0.72
Southeast and East Asia	TC-DT	+0.41	+0.14	-1.84	+1.15	-4.32	-4.14	+0.13	+2.68	-1.20	-1.44
	DT	-0.83	-0.90	+0.01	+0.67	-0.71	-0.71	+0.96	+2.05	-0.30	-0.36
	proportion	+0.56	+1.71	+1.27	+1.73	-4.31	-3.64	+0.07	+1.99	-1.10	-1.22
North and Central America	TC-DT	-1.82	+0.33	-9.87	-4.62	+0.88	-0.12	-0.70	-4.57	+0.58	+0.13
	DT	-1.75	-0.98	-6.68	-4.14	-0.80	-0.70	-2.74	-3.54	-0.22	-0.59
	proportion	+0.01	+1.14	-2.25	-2.05	+2.13	-0.05	+2.23	-2.69	+1.10	+0.72
Australia	TC-DT	+1.26	-1.78	+2.07	-1.44	+1.63	+0.15	+12.99	+0.18	+0.41	-0.11
	DT	+1.16	+0.30	+2.28	-1.46	-1.92	-1.72	+5.44	+1.04	-0.32	-0.05
	proportion	+2.57	-4.01	+2.14	-1.57	+2.35	-0.23	+8.80	-2.62	+0.39	-0.53

+2.22/-0.90 slope of the trend(%)

- significant increase ($p<0.01$)
- significant increase ($p<0.05$)
- non-significant increase ($p>0.05$)
- significant decrease ($p<0.01$)
- significant decrease ($p<0.05$)
- non-significant decrease ($p>0.05$)

Fig. 6 | Trends in the concurrences of TC rainfall and drought terminations. Numbers in the grids show the changing rate (% per year) of the number of drought termination (DT) events and those caused by high rainfall (TC-DT), and the proportion of the number of TC-DT events to the total DT events. The changing rate is derived from the Poisson regression of the number of TC-DT and DT events, and the proportion value of the number of TC-DT events to those of the DT events. Color filled grids show the changing rate is statistically significant, while the unfilled frames show that the changing rate in those grids are not statistically significant. Orange and blue colors show increases and decreases, respectively. Each column shows values derived from SPI of two-time scales (SPI-6 and SPI-12) using specific precipitation datasets (CMORPH, PERSIANN-CDR, and ERA5-Land) of specific time periods (1999–2021, 1985–2022, and 195–2022). Each row shows values for a variable (the number of TC-DT and DT events, and the proportion of the number of TC-DT to DT events as well) in the four hotspot regions shown in Figs. 3, 4, including the Arabian Peninsula and South Asia, the Southeast and East Asia, the east and west of North and Central America, and the northwest of Australia.

hourly accumulated precipitation from 1950 to present day worldwide with a resolution of $0.1 \times 0.1°$[35].

Satellite precipitation products tend to overestimate precipitation in arid climates and underestimate it in humid climates[54], and are particularly prone to bias in semiarid continental regions during the warm season[55]. As a high-resolution precipitation dataset, CMORPH demonstrates superior performance in capturing spatiotemporal patterns across most global regions[56,57]. In studies of humid areas in southern China, CMORPH outperforms PERSIANN and CHIRPS in extreme precipitation estimates[58], but tends to overestimate warm-season rainfall in the United States and underestimate rainfall in the tropical Pacific[57]. In multiscale assessments, CMORPH's estimates of maximum 5-day precipitation are the best among all products, but there are still large biases in extreme precipitation estimates[59]. In global assessments, PERSIANN-CDR has limited ability to capture extreme precipitation in some regions, especially in terms of precipitation extreme indices[60]. In studies of complex terrain and humid areas in southern China, PERSIANN-CDR performs well on daily and monthly scales, but there is a tendency to underestimate precipitation events[61].

Satellite precipitation products can accurately detect drought events in drought-related climates[54]. CMORPH performs well in drought assessment in the Yellow River Basin of China, and the results are consistent with ground-based meteorological data[62]. PERSIANN-CDR data have good drought event detection capabilities in arid and semi-arid climates, especially on longer time scales[54], but biases in precipitation lead to a certain false alarm rate[63]. PERSIANN-CDR may underestimate precipitation in study areas (such as Iran)[64], so the number of drought events observed using the SPI index on longer time scales (>6 months) is more consistent with observations than the shorter time scales (SPI-1 and SPI-3)[65]. Therefore, in this study, we used these two observed precipitation datasets for calculating SPI-6 and SPI-12 to detect droughts, with the reanalysis ERA5-Land as a reference for long-term changes in TC rainfall. The uncertainties resulting from the precipitation datasets are comprehensively examined for this study.

TC observations were obtained from IBTrACS[28], providing six-hourly TC track and intensity records. More intense TCs tend to have greater rainfall rates than weaker TCs[52,66]. Moreover, TCs that decay more slowly tend to produce more intense precipitation[67]. Additionally,
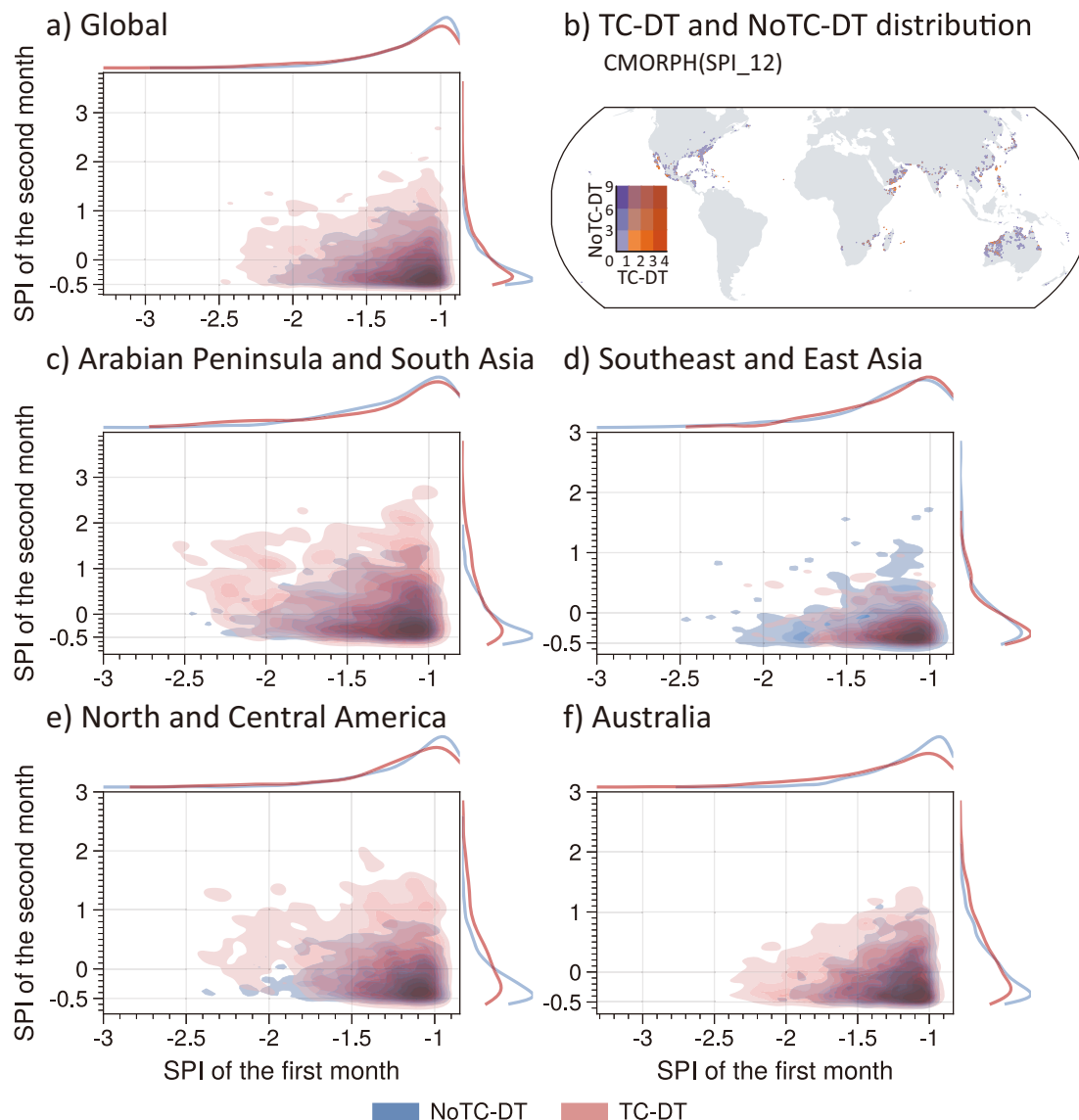
Fig. 7 | Transitions of drought regimes with the drought termination. Subplots **a**, **c**–**f** show the probability density distribution of SPI values of the first and second months of NoTC-DT (blue) and TC-DT (red) events for global and four hotspots (**a**, **c**–**f**). NoTC-DT and TC-DT events are shorted for the drought termination events caused by no-high TC precipitation and high TC rainfall, respectively. Subplot b shows the spatial distribution of the number of NoTC-DT and TC-DT events. Results are derived from SPI-12 using CMORPH precipitation dataset.

Surface winds are rapidly weakened within 12 h after TC landfalling, due to increases in surface roughness and enthalpy fluxes. When a TC weakens to be a tropical storm, the TC intensity weakens slowly[68]. To capture the comprehensive impacts of TCs on drought, TCs considered in this study consist of TCs with maximum sustained winds of 64 knots or higher, tropical storms (>33 knots), and tropical depressions (≤33 knots) in IBTrACS TC track records.

We used six-hourly TC track point data to identify the area affected by TCs. A grid within the circle of 500 km radius centered on a TC track point is considered to be confronted with TC impacts at a time. If a grid is impacted by n TC track points, it is considered that the grid has undergone n times of TC impacts. By separating the values of n composite from all grids of n larger than 0, we classified regions impacted by TCs to regions of severe, high, middle, and low impacts (Supplementary Fig. 7). If a grid experienced at least a time of TC impact in a day, the precipitation in that day for that grid is identified as TC rainfall. A radius threshold of 500 km is sufficiently large to encompass all TC rainfall and has been commonly adopted for TC rainfall identification[69]. A radius threshold larger than 500 km cannot improve TC

rainfall identification[4,51,52], so our TCP identification is reasonable for TC impact analyses.

Drought termination

We used the SPI[70] to identify drought and DT events. SPI enables the identification of meteorological drought conditions at a specified time scale of interest. SPI computation at long time scales can consider preceding hydroclimatic conditions, thus allowing the index to retain memory of precipitation deficit over previous months. A large monthly SPI shift indicates noteworthy transitions between wetness and dryness. We defined the drought as a monthly SPI value of ≤ −1.0 at 12-month time scale. The drought identified for DT event identification should be a long-term cumulative meteorological outcome rather than a short-lived dry-wet fluctuation, so we calculate SPI using the 6-month and 12-month time scales for short- and long-droughts, respectively.

We define a DT event as one or more successive months of drought followed immediately by a month with an SPI value of ≥ −0.5 (indicating near-normal or wetter conditions). A climatological transition at the end of
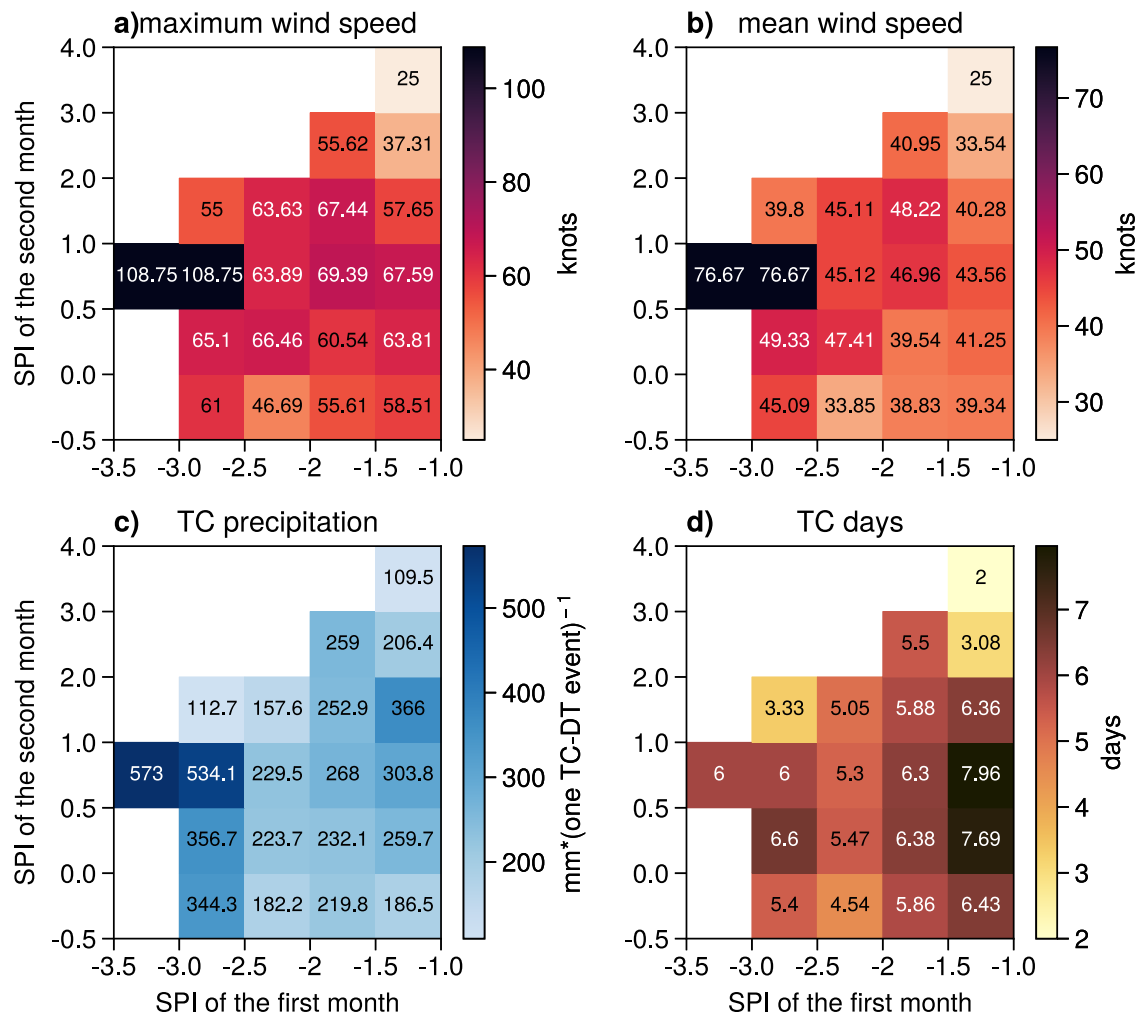
Fig. 8 | Transition of meteorological conditions in TC-DT events. Distribution of the maximum wind speed (**a**), mean wind speed (**b**), TC precipitation (**c**), and TC times (**d**) in different magnitude TC-DT events.

a drought event from the first month of SPI < -1.0 to the following month of SPI larger than -0.5 is regarded as a DT event. We then focus on precipitation in the month of drought relief and the month of a DT event. We aggregate rainfall resulting from TCs within these 2 months. If the combined contribution of TC rainfall exceeds 50% of the total precipitation for these 2 months in a DT event, we categorize that DT event as being predominantly influenced by TC rainfall, defining it as a TC-related DT (TC-DT) event. To identify the importance of TC rainfall to global drought, we identify the percentage of TC-DT events to the total drought events for each year. Changes in the percentage of TC-DT events annually are analyzed by the Poisson regression and the significance of trends is detected by the Mann–Kendall test.

To validate the definition of drought events on the robustness of our analyses results, we further conducted the same analyses using the definition of a DT event as three or more than three successive months of drought followed immediately by a month with an SPI value of ≥ -0.5 (indicating near-normal or wetter conditions). This definition inevitably results in less DT events, as shown in comparison between Fig. 5 and Supplementary Fig. 3, as well as between Fig. 6 and Supplementary Fig. 4, but increases in the occurrences of TC-DT events are similar in the global and regional scales. Most regions even show higher dependency on TC to terminate droughts lasting longer duration, except North and Central America.

The original temporal coverages of the PERSIANN-CDR and CMORPH datasets are 1983–2022 and 1998–2021, respectively. When using them to calculate the SPI-6 and SPI-12 indices, there is no data obtained for the first 5 (11) months of SPI-6 (SPI-12) due to the aggregation

of precipitation time series to the target time scales for SPI. To make the trend analyses consistently, we only considered years of complete SPI data and thus removed data for in the first year, including the missing SPI derived from each dataset. Additionally, the PERSIANN-CDR dataset exhibits a low sample size for TC-DT events in 1984, possibly due to the unrecorded TCs, which may affect the overall trend analysis. Therefore, the values for 1984 derived from the PERSIANN-CDR dataset are excluded as uncertain outliers. Consequently, to investigate changes in the TC-DT events, the study periods are set to 1985–2022 and 1999–2021 for PERSIANN-CDR and CMORPH datasets, respectively. We complementarily conducted similar analyses using the ERA5-Land precipitation dataset to validate the results and make the conclusion more robust. The result of the first year of 1950 was also removed, and thus the study period for the analyses using the ERA5-Land is 1951–2022.

Event coincidence analysis
To further assess the impacts of TC rainfall on the occurrence of DT events, we conduct the event coincidence analysis (ECA)[71], incorporated in the "CoinCalc" R package[72], and evaluate the relationship between TC rainfall and DT events. ECA has been widely adopted for causal analyses within the fields of meteorology[73], hydrometeorology[74], and social sciences[71]. Recently, ECA has been applied to identify potential drivers of DT in the British–Irish Isles[22].

ECA analyzes two binary time series of events that are hypothesized to be associated. In this analysis, event series "A" represents the binary DT series which shows whether DT occurs in a month, and event series "B"

represents the binary TCP time series, which show whether TC precipitation amounts to 50% of the total precipitation in the 2 months. We set n to indicate the order of a month in the overall time series. If the $SPI_n \leq -1.0$ and the $SPI_{n+1} \geq -0.5$, $A_n = 1$, otherwise $A_n = 0$. The portion of TC rainfall to the total precipitation (P) for a month n is $portion_n = \frac{TCP_n + TCP_{n+1}}{P_n + P_{n+1}}$ (n is less than the length of event series B). If $portion_n \geq 0.5$, $B_n = 1$, otherwise $B_n = 0$.

A tolerance window $\triangle T$ is applied to detect occurrences of high TC rainfall preceding DT. $\triangle T$ enables the consideration of uncertain timings of DT events. We have already located the high TC rainfall and DT events in specific months, so we take $\triangle T = 0$. ECA estimates the precursor coincidence rate to evaluate all instances of DT events and assesses how many are preceded by high TC rainfall. The precursor coincidence rate $= 1 (= 0)$ indicates that every (no) DT event is preceded by high TC rainfall. The statistical significance of the precursor coincidence rate is tested by the Shuffle test, in which the significance equates to a greater number of occurrences than expected by chance.

Data availability
CMORPH dataset is obtained from https://www.ncei.noaa.gov/products/climate-data-records/precipitation-cmorph. PERSIANN-CDR dataset is available at https://www.ncdc.noaa.gov/cdr/atmospheric/precipitation-persiann-cdr. IBTrACS dataset is available at https://www.ncei.noaa.gov/products/international-best-track-archive?name=sources. ERA5-Land is available at https://cds.climate.copernicus.eu/datasets/reanalysis-era5-land?tab=download.

Code availability
The codes and source data necessary to reproduce all the figures in this study, can be found in the following Zenodo repository: https://doi.org/10.5281/zenodo.13848266.

References
1. Rappaport, E. N. Fatalities in the United States from Atlantic tropical cyclones: new data and interpretation. *Bull. Am. Meteorol. Soc.* **95**, 341–346 (2014).
2. Iglesias, V. et al. Risky development: increasing exposure to natural hazards in the United States. *Earth's Future* **9**, e2020EF001795 (2021).
3. Klotzbach, P. J., Bowen, S. G., Pielke, R. & Bell, M. Continental U.S. hurricane landfall frequency and associated damage: observations and future risks. *Bull. Am. Meteorol. Soc.* **99**, 1359–1376 (2018).
4. Touma, D., Stevenson, S., Camargo, S. J., Horton, D. E. & Diffenbaugh, N. S. Variations in the intensity and spatial extent of tropical cyclone precipitation. *Geophys. Res. Lett.* **46**, 13992–14002 (2019).
5. Vink, K. & Md. Ahsan, N. The benefits of cyclones: a valuation approach considering ecosystem services. *Ecol. Indic.* **95**, 260–269 (2018.
6. Vo, T.-H. & Liou, Y.-A. Tropical cyclone-induced rainfall variability and its implications for drought in Taiwan: insights from 1981 to 2022. *Atmos. Res.* **312**, 107771 (2024).
7. Fedorov, A. V., Brierley, C. M. & Emanuel, K. Tropical cyclones and permanent El Niño in the early Pliocene epoch. *Nature* **463**, 1066–1070 (2010).
8. Conner, W. H., Day, J. W., Baumann, R. H. & Randall, J. M. Influence of hurricanes on coastal ecosystems along the northern Gulf of Mexico. *Wetl. Ecol. Manag.* **1**, 45–56 (1989).
9. Pérez-Alarcón, A. et al. Impacts of tropical cyclones on the global water budget. *npj Clim. Atmos. Sci.* **6**, 1–9 (2023).
10. Song, J. Y., Abbaszadeh, P., Deb, P. & Moradkhani, H. Unraveling the relationship between tropical storms and agricultural drought. *Earth's Future* **10**, https://doi.org/10.1029/2021EF002417 (2022).
11. Jing, Y., Li, J., Weng, Y. & Wang, J. The assessment of drought relief by typhoon Saomai based on MODIS remote sensing data in Shanghai, China. *Nat. Hazards* **71**, 1215–1225 (2014).
12. Maxwell, J. T., Ortegren, J. T., Knapp, P. A. & Soulé, P. T. Tropical cyclones and drought amelioration in the Gulf and Southeastern Coastal United States. *J. Clim.* **26**, 8440–8452 (2013).
13. Gao, Y. et al. Spatiotemporal links between meteorological and agricultural droughts impacted by tropical cyclones in China. *Sci. Total Environ.* **912**, 169119 (2023).
14. Tan, X. et al. Increasing global precipitation whiplash due to anthropogenic greenhouse gas emissions. *Nat. Commun.* **14**, 2796 (2023).
15. Parry, S., Prudhomme, C., Wilby, R. L. & Wood, P. J. Drought termination: concept and characterisation. *Prog. Phys. Geogr.* **40**, 743–767 (2016).
16. Schwalm, C. R. et al. Global patterns of drought recovery. *Nature* **548**, 202–205 (2017).
17. Maxwell, J. T., Knapp, P. A., Ortegren, J. T., Ficklin, D. L. & Soulé, P. T. Changes in the mechanisms causing rapid drought cessation in the Southeastern United States. *Geophys. Res. Lett.* **44**, 12,476–12,483 (2017).
18. Zhang, W., Zhou, T. & Wu, P. Anthropogenic amplification of precipitation variability over the past century. *Science* **385**, 427–432 (2024).
19. Qiao, Y., Xu, W., Meng, C., Liao, X. & Qin, L. Increasingly dry/wet abrupt alternation events in a warmer world: observed evidence from China during 1980–2019. *Int. J. Climatol.* **42**, 6429–6440 (2022).
20. Chen, H. & Wang, S. Accelerated transition between dry and wet periods in a warming climate. *Geophys. Res. Lett.* **49**, e2022GL099766 (2022).
21. Maxwell, J. T., Soulé, P. T., Ortegren, J. T. & Knapp, P. A. Drought-busting tropical cyclones in the Southeastern Atlantic United States: 1950–2008. *Ann. Assoc. Am. Geogr.* **102**, 259–275 (2012).
22. Parry, S. et al. Abrupt drought termination in the British–Irish Isles driven by high atmospheric vapour transport. *Environ. Res. Lett.* **18**, 104050 (2023).
23. Knutson, T. et al. Tropical cyclones and climate change assessment: part I: detection and attribution. *Bull. Am. Meteorol. Soc.* **100**, 1987–2007 (2019).
24. Jing, R. et al. Global population profile of tropical cyclone exposure from 2002 to 2019. *Nature* **626**, 549–554 (2024).
25. YuXin, J., JiaPeng, L. & Yuan, W. Effect of tropical cyclone precipitation on alleviating the drought situation in the southeast coastal regions of China during summer and autumn: using the improved objective synoptic analysis technique. *J. Trop. Meteorol.* **22**, 277–286 (2016).
26. Kossin, J. P., Emanuel, K. A. & Vecchi, G. A. The poleward migration of the location of tropical cyclone maximum intensity. *Nature* **509**, 349–352 (2014).
27. Cao, X. et al. The projected poleward shift of tropical cyclogenesis at a global scale under climate change in MRI-AGCM3.2H. *Geophys. Res. Lett.* **51**, e2023GL107189 (2024).
28. Knapp, K. R., Kruk, M. C., Levinson, D. H., Diamond, H. J. & Neumann, C. J. The international best track archive for climate stewardship (IBTrACS): unifying tropical cyclone data. *Bull. Am. Meteorol. Soc.* **91**, 363–376 (2010).
29. Moon, I.-J., Kim, S.-H. & Chan, J. C. L. Climate change and tropical cyclone trend. *Nature* **570**, E3–E5 (2019).
30. Emanuel, K. Limitations of reanalyses for detecting tropical cyclone trends. *Nat. Clim. Change* 1–3, https://doi.org/10.1038/s41558-023-01879-y (2023).
31. Chand, S. S. et al. Declining tropical cyclone frequency under global warming. *Nat. Clim. Change* **12**, 655–661 (2022).
32. Zhao, H. et al. Decreasing global tropical cyclone frequency in CMIP6 historical simulations. *Sci. Adv.* **10**, eadl2142 (2024).

33. Joyce, R. J., Janowiak, J. E., Arkin, P. A. & Xie, P. CMORPH: a method that produces global precipitation estimates from passive microwave and infrared data at high spatial and temporal resolution. *J. Hydrometeorol.* **5**, 487–503 (2004).

34. Ashouri, H. et al. PERSIANN-CDR: daily precipitation climate data record from multisatellite observations for hydrological and climate studies. *Bull. Am. Meteorol. Soc.* **96**, 69–83 (2015).

35. Muñoz-Sabater, J. et al. ERA5-Land: a state-of-the-art global reanalysis dataset for land applications. *Earth Syst. Sci. Data* **13**, 4349–4383 (2021).

36. Bhatia, K. et al. A potential explanation for the global increase in tropical cyclone rapid intensification. *Nat. Commun.* **13**, 6626 (2022).

37. Qin, L. et al. Global expansion of tropical cyclone precipitation footprint. *Nat. Commun.* **15**, 4824 (2024).

38. Camargo, S. J., Sobel, A. H., Barnston, A. G. & Klotzbach, P. J. The influence of natural climate variability on tropical cyclones, and seasonal forecasts of tropical cyclone activity. in *World Scientific Series on Asia-Pacific Weather and Climate,* Vol. 4, 325–360 (WORLD SCIENTIFIC, 2010).

39. Gray, W. M. Global view of the origin of tropical disturbances and storms. *Mon. Weather Rev.* **96**, 669–700 (1968).

40. Liu, L., Huang, Y. & Liu, L. Comparative analysis of the rapid intensification of two super cyclonic storms in the Arabian Sea. *Trop. Cyclone Res. Rev.* **13**, 41–54 (2024).

41. Dettinger, M. D. Atmospheric rivers as drought busters on the U.S. West Coast. *J. Hydrometeorol.* **14**, 1721–1732 (2013).

42. Prat, O. P. & Nelson, B. R. On the link between tropical cyclones and daily rainfall extremes derived from global satellite observations. *J. Clim.* **29**, 6127–6135 (2016).

43. Zhao, M. A Study of AR-, TS-, and MCS-associated precipitation and extreme precipitation in present and warmer climates. *J. Clim.* **35**, 479–497 (2022).

44. Kam, J., Sheffield, J., Yuan, X. & Wood, E. F. The influence of Atlantic tropical cyclones on drought over the eastern United States (1980–2007). *J. Clim.* **26**, 3067–3086 (2013).

45. Brun, J. & Barros, A. P. Mapping the role of tropical cyclones on the hydroclimate of the Southeast United States: 2002–2011. *Int. J. Climatol.* **34**, 494–517 (2014).

46. Prodhan, F. A., Zhang, J., Hasan, S. S., Pangali Sharma, T. P. & Mohana, H. P. A review of machine learning methods for drought hazard monitoring and forecasting: current research trends, challenges, and future research directions. *Environ. Model. Softw.* **149**, 105327 (2022).

47. Culley, S. et al. A bottom-up approach to identifying the maximum operational adaptive capacity of water resource systems to a changing climate. *Water Resour. Res.* **52**, 6751–6768 (2016).

48. Ortiz, A. M. D. et al. Impacts of tropical cyclones on food security, health and biodiversity. *Bull. World Health Organ.* **101**, 152–154 (2023).

49. Guzman, O. & Jiang, H. Heavier inner-core rainfall of major hurricanes in the North Atlantic basin than other global basins. *J. Clim.* 1–35, https://doi.org/10.1175/jcli-d-20-0668.1 (2021).

50. Tan, X., Wu, X. & Liu, B. Global changes in the spatial extents of precipitation extremes. *Environ. Res. Lett.* **16**, 054017 (2021).

51. Wu, X., Tan, X., Liu, B., Chen, H. & Chen, X. Fronts and cyclones associated with changes in the total and extreme precipitation over China. *J. Clim.* **35**, 4131–4146 (2022).

52. Tan, X., Liu, Y., Wu, X., Liu, B. & Chen, X. Examinations on global changes in the total and spatial extent of tropical cyclone precipitation relating to rapid intensification. *Sci. Total Environ.* **853**, 158555 (2022).

53. Xie, P. et al. Reprocessed, bias-corrected CMORPH global high-resolution precipitation estimates from 1998. *J. Hydrometeorol.* **18**, 1617–1641 (2017).

54. Kazemzadeh, M. et al. Detecting drought events over Iran during 1983–2017 using satellite and ground-based precipitation observations. *Atmos. Res.* **269**, 106052 (2022).

55. Rosenfeld, D. & Mintz, Y. Evaporation of rain falling from convective clouds as derived from radar measurements. *J. Appl. Meteorol.* **27**, 209–215 (1988).

56. Xie, P. et al. A gauge-based analysis of daily precipitation over East Asia. *J. Hydrometeorol.* **8**, 607–626 (2007).

57. Sapiano, M. R. P. & Arkin, P. A. An intercomparison and validation of high-resolution satellite precipitation estimates with 3-hourly gauge data. *J. Hydrometeorol.* **10**, 149–166 (2009).

58. Wang, Q. et al. Assessment of four latest long-term satellite-based precipitation products in capturing the extreme precipitation and streamflow across a humid region of southern China. *Atmos. Res.* **257**, 105554 (2021).

59. Zhang, T., Yang, Y., Dong, Z. & Gui, S. A multiscale assessment of three satellite precipitation products (TRMM, CMORPH, and PERSIANN) in the Three Gorges Reservoir area in China. *Adv. Meteorol.* **2021**, 1–27 (2021).

60. Nguyen, P. et al. Evaluation of CMIP5 model precipitation using PERSIANN-CDR. *J. Hydrometeorol.* **18**, 2313–2330 (2017).

61. Shaowei, N. et al. Comprehensive evaluation of satellite-derived precipitation products considering spatial distribution difference of daily precipitation over eastern China. *J. Hydrol.* **44**, 101242 (2022).

62. Wang, F., Yang, H., Wang, Z., Zhang, Z. & Li, Z. Drought evaluation with CMORPH satellite precipitation data in the yellow river basin by using gridded standardized precipitation evapotranspiration index. *Remote Sens.* **11**, 485 (2019).

63. Helmi, A. M. & Abdelhamed, M. S. Evaluation of CMORPH, PERSIANN-CDR, CHIRPS V2.0, TMPA 3B42 V7, and GPM IMERG V6 satellite precipitation datasets in Arabian arid regions. *Water* **15**, 92 (2023).

64. Alijanian, M., Rakhshandehroo, G. R., Mishra, A. K. & Dehghani, M. Evaluation of satellite rainfall climatology using CMORPH, PERSIANN-CDR, PERSIANN, TRMM, MSWEP over Iran. *Int. J. Climatol.* **37**, 4896–4914 (2017).

65. Alijanian, M., Rakhshandehroo, G. R., Mishra, A. & Dehghani, M. Evaluation of remotely sensed precipitation estimates using PERSIANN-CDR and MSWEP for spatio-temporal drought assessment over Iran. *J. Hydrol.* **579**, 124189 (2019).

66. Lavender, S. L. & McBride, J. L. Global climatology of rainfall rates and lifetime accumulated rainfall in tropical cyclones: influence of cyclone basin, cyclone intensity and cyclone size. *Int. J. Climatol.* **41**, E1217–E1235 (2021).

67. Lai, Y. et al. Slower-decaying tropical cyclones produce heavier precipitation over China. *npj Clim. Atmos. Sci.* **7**, 1–13 (2024).

68. Hlywiak, J. & Nolan, D. S. The response of the near-surface tropical cyclone wind field to inland surface roughness length and soil moisture content during and after landfall. *J. Atmos. Sci.* **78**, 983–1000 (2021).

69. Shen, Z.-Q., Nie, G.-Z., Qiu, X., Gu, J.-F. & Zhang, Y. Outer size distribution of landfalling tropical cyclones over China changes in the recent decades. *J. Clim.* **36**, 6427–6445 (2023).

70. Mckee, T. B., Doesken, N. J. & Kleist, J. The relationship of drought frequency and duration to time scales. In *Proc. 8th Conference on Applied Climatology*, 179–183 (American Meteorological Society, 1993).

71. Donges, J. F., Schleussner, C.-F., Siegmund, J. F. & Donner, R. V. Event coincidence analysis for quantifying statistical interrelationships between event time series. *Eur. Phys. J. Spec. Top.* **225**, 471–487 (2016).

72. Siegmund, J. F., Wiedermann, M., Donges, J. F. & Donner, R. V. Impact of temperature and precipitation extremes on the flowering dates of four German wildlife shrub species. *Biogeosciences* **13**, 5541–5555 (2016).

73. Raymond, C. et al. Understanding and managing connected extreme events. *Nat. Clim. Change* **10**, 611–621 (2020).

74. Chen, Y., Liao, Z., Shi, Y., Tian, Y. & Zhai, P. Detectable increases in sequential flood-heatwave events across China during 1961–2018. *Geophys. Res. Lett.* **48**, https://doi.org/10.1029/2021gl092549 (2021).

Author contributions
Xuezhi Tan: conceptualization, methodology, supervision. Yaxin Liu: formal analysis, writing—original draft. Xinxin Wu: data curation, validation. Xuejin Tan: investigation, visualization. Chengguang Lai: resources. Huabin Shi: software, code development. Thian Yew Gan: funding acquisition, project administration. All authors contributed to writing—review & editing.

Competing interests
The authors declare no competing interests.

Additional information
Supplementary information The online version contains supplementary material available at https://doi.org/10.1038/s43247-025-02564-y.

Correspondence and requests for materials should be addressed to Xuezhi Tan.

Peer review information *Communications Earth & Environment* thanks Christian Dominguez and the other anonymous reviewer(s) for their contribution to the peer review of this work. Primary Handling Editor: Alireza Bahadori. A peer review file is available.

Reprints and permissions information is available at http://www.nature.com/reprints

Publisher's note Springer Nature remains neutral with regard to jurisdictional claims in published maps and institutional affiliations.